
Ensemble Bayesian Optimization

Zi Wang[†] Clement Gehring[†] Pushmeet Kohli[‡] Stefanie Jegelka[†]

[†] MIT CSAIL {ziw, gehring, stefje}@csail.mit.edu

[‡] DeepMind pushmeet@google.com

Abstract

Bayesian Optimization (BO) has been shown to be a very effective paradigm for tackling hard black-box and non-convex optimization problems encountered in Machine Learning. Despite these successes, the computational complexity of the underlying function approximation has restricted the use of BO to problems that can be handled with less than a few thousand function evaluations. Harder problems like those involving functions operating in very high dimensional spaces may require hundreds of thousands or millions of evaluations or more and become computationally intractable to handle using standard Bayesian Optimization methods. In this paper, we propose Ensemble Bayesian Optimization (EBO) to overcome this problem. Unlike conventional BO methods that operate on a single posterior GP model, EBO works with an ensemble of posterior GP models. Further, we represent each GP model using tile coding random features and an additive function structure. Our approach generates speedups by parallelizing the time consuming hyper-parameter posterior inference and functional evaluations on hundreds of cores and aggregating the models in every iteration of BO. Our extensive experimental evaluation shows that EBO can speed up the posterior inference between 2-3 orders of magnitude (400 times in one experiment) compared to the state-of-the-art by putting data into Mondrian bins without sacrificing the sample quality. We demonstrate the ability of EBO to handle sample-intensive hard optimization problems by applying it to a rover navigation problem with tens of thousands of observations.

1 Introduction

Global optimization of black-box and non-convex functions is an important component of modern machine learning. From optimizing hyperparameters in deep models to solving inverse problems encountered in computer vision and policy search for reinforcement learning, these optimization problems have many important applications in machine learning and its allied disciplines. In the past decade, Bayesian optimization has become a popular approach for global optimization of non-convex functions that are expensive to evaluate. Recent work addresses better query strategies [16, 20, 26, 11, 12, 14, 29, 15, 28], techniques for batch queries [6, 7, 10, 31], and algorithms for high dimensional problems [32, 8, 18, 13, 31].

Despite the above-mentioned successes, Bayesian optimization remains somewhat impractical, since it is typically coupled with expensive function estimators (Gaussian processes) and non-convex acquisition functions that are hard to optimize in high dimensions and sometimes expensive to evaluate. To alleviate these difficulties, recent work explored the use of random feature approximations [25, 17] and sparse Gaussian processes [19], but, while improving scalability, these methods still suffer from misestimation of confidence bounds (an essential part of the acquisition functions), and expensive/inaccurate Gaussian process (GP) hyperparameter inference. Indeed, to the best of our knowledge, Bayesian optimization is typically limited to a few thousand evaluations [17]. Yet, reliable search and estimation for complex functions in very high-dimensional spaces may well

Under review.

require more evaluations. Comparing to the millions of evaluations possible (and needed) with *local* methods like stochastic gradient descent, the scalability of *global* Bayesian optimization leaves large room for desirable progress. In particular, the lack of scalable uncertainty estimates to guide the search is a major roadblock for huge-scale Bayesian optimization.

In this paper, we propose ensemble Bayesian optimization (EBO), a global optimization method targeted to high dimensional, large scale parameter search problems whose queries are parallelizable. Such problems are abundant in hyper- and control parameter optimization in machine learning and robotics [5, 24]. EBO relies on two main ideas that are implemented at multiple levels: (1) we use efficient partition-based function approximators (across data and features) that simplify and accelerate search and optimization; (2) we enhance the expressive power of these approximators by using ensembles and a stochastic approach. We maintain an evolving (posterior) distribution over the (infinite) ensemble and, in each iteration, draw one member to perform search and estimation.

For improved GP estimation, we propose a novel hierarchical additive GP model based on tile coding (a.k.a. random binning or Mondrian forest features). We learn a posterior distribution over kernel width and the additive structure; here, Gibbs sampling prevents overfitting. To accelerate the sampler, which depends on the likelihood of the observations, we use an efficient, randomized block approximation of the Gram matrix based on a Mondrian process. Parallelizing sampling and query selection can then be parallelized across blocks, further speeding up the algorithm.

As a whole, this combination of simple, tractable structure with ensemble learning and randomization improves efficiency, uncertainty estimates and optimization. Moreover, our realization of these ideas offers an alternative explanation for global optimization heuristics that have been popular in other communities, indicating possible directions for further theoretical analysis. Our empirical results demonstrate that EBO can speed up the posterior inference between 2-3 orders of magnitude (400 times in one experiment) compared to the state-of-the-art without sacrificing the sample quality. Furthermore, we demonstrate the ability of EBO to handle sample-intensive hard optimization problems by applying it on a rover navigation problem with tens of thousands of observations.

2 Background and Challenges

Consider a simple but high dimensional search space $\mathcal{X} = [0, R]^D \subseteq \mathbb{R}^D$. We aim to find a maximizer $x^* \in \arg \max_{x \in \mathcal{X}} f(x)$ of an unknown function $f : \mathcal{X} \rightarrow \mathbb{R}$.

Gaussian processes Gaussian processes (GPs) are popular priors for modeling the function f in Bayesian optimization. They define distributions over functions where any finite set of function values has a multivariate Gaussian distribution. A Gaussian process $\mathcal{GP}(\mu, \kappa)$ is fully specified by a mean function $\mu(\cdot)$ and covariance (kernel) function $\kappa(\cdot, \cdot)$. Let f be a function sampled from $\mathcal{GP}(0, \kappa)$. Given the observations $\mathcal{D}_n = \{(\mathbf{x}_t, y_t)\}_{t=1}^n$ where $y_t \sim \mathcal{N}(f(\mathbf{x}_t), \sigma)$, we obtain the posterior mean and variance

$$\mu_n(\mathbf{x}) = \boldsymbol{\kappa}_n(\mathbf{x})^\top (\mathbf{K}_n + \sigma^2 \mathbf{I})^{-1} \mathbf{y}_n, \quad \sigma_n^2(\mathbf{x}) = \kappa(\mathbf{x}, \mathbf{x}) - \boldsymbol{\kappa}_n(\mathbf{x})^\top (\mathbf{K}_n + \sigma^2 \mathbf{I})^{-1} \boldsymbol{\kappa}_n(\mathbf{x}) \quad (2.1)$$

of the function via the kernel matrix $\mathbf{K}_n = [\kappa(\mathbf{x}_i, \mathbf{x}_j)]_{\mathbf{x}_i, \mathbf{x}_j \in \mathcal{D}_n}$ and $\boldsymbol{\kappa}_n(\mathbf{x}) = [\kappa(\mathbf{x}_i, \mathbf{x})]_{\mathbf{x}_i \in \mathcal{D}_n}$ [22]. The log data likelihood for \mathcal{D}_n is given by

$$\log p(\mathcal{D}_n) = -\frac{1}{2} \mathbf{y}_n^\top (\mathbf{K}_n + \sigma^2 \mathbf{I})^{-1} \mathbf{y}_n - \frac{1}{2} \log |\mathbf{K}_n + \sigma^2 \mathbf{I}| - \frac{n}{2} \log 2\pi. \quad (2.2)$$

While GPs provide flexible, broadly applicable function estimators, the $O(n^3)$ computation of the inverse $(\mathbf{K}_n + \sigma^2 \mathbf{I})^{-1}$ and determinant $|\mathbf{K}_n + \sigma^2 \mathbf{I}|$ can become major bottlenecks as n grows, for both posterior function value predictions and data likelihood estimation.

Additive structures To reduce the complexity of the vanilla GP, we assume a latent decomposition of the input dimensions $[D] = \{1, \dots, D\}$ into disjoint subspaces, namely, $\bigcup_{m=1}^M A_m = [D]$ and $A_i \cap A_j = \emptyset$ for all $i \neq j, i, j \in [M]$. As a result, the function f decomposes as $f(x) = \sum_{m \in [M]} f_m(x^{A_m})$ [13]. If each component f_m is drawn independently from $\mathcal{GP}(\mu^{(m)}, \kappa^{(m)})$ for all $m \in [M]$, the resulting f will also be a sample from a GP: $f \sim \mathcal{GP}(\mu, \kappa)$, with priors $\mu(x) = \sum_{m \in [M]} \mu_m(x^{A_m}), \quad \kappa(x, x') = \sum_{m \in [M]} \kappa^{(m)}(x^{A_m}, x'^{A_m})$.

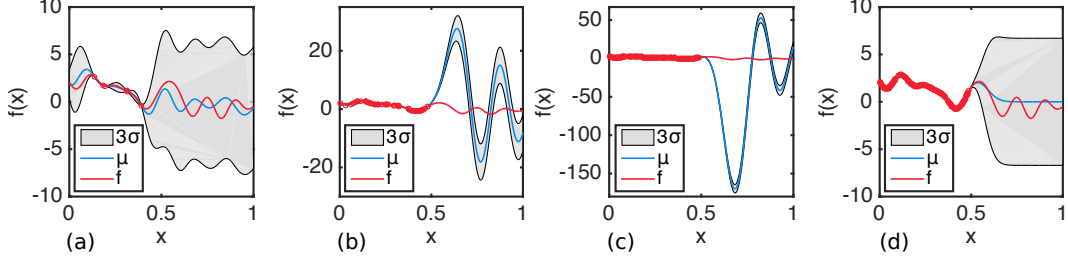


Figure 1: We use 1000 Fourier features [21] to approximate a 1-dimensional GP with zero mean and squared exponential kernel. The observations are samples from a function f (red line) drawn from the GP. (a) We sample 100 observations (red circles) from $[-10, 0.5]$. The Fourier features are able to predict reasonable confidence bounds. (b) We sample 1000 observations from $[-10, 0.5]$. (c) We sample 5000 observations from $[-10, 0.5]$. The scale of the variance predictions are very small compared to the mean predictions. (d) The ground truth predictions of the original GP conditioned on the same 5000 observations as (c). Variance starvation becomes a serious problem for random features when the size of data is close to or larger than the size of the features.

The additive structure helps BO to search more efficiently and effectively, but it remains challenging to learn a good decomposition structure $\{A_m\}$. Recently, Wang et al. [31] proposed learning via Gibbs sampling. This Gibbs sampler takes hours for merely a few hundred points, because it needs a vast number of expensive data likelihood computations.

Random features It is possible use random features [21] to approximate the GP kernel and alleviate the $O(n^3)$ computation in Eq. (2.1) and Eq. (2.2). Let $\phi : \mathcal{X} \mapsto \mathbb{R}^{D_R}$ be the (scaled) random feature operator and $\Phi_n = [\phi(\mathbf{x}_1), \dots, \phi(\mathbf{x}_n)]^T \in \mathbb{R}^{n \times D_R}$. The GP posterior mean and variance become

$$\mu_n(\mathbf{x}) = \phi(\mathbf{x})^T \Phi_n^T (\Phi_n \Phi_n^T + \sigma^2 \mathbf{I})^{-1} \mathbf{y}_n, \quad (2.3)$$

$$\sigma_n^2(\mathbf{x}) = \phi(\mathbf{x})^T \phi(\mathbf{x}) - \phi(\mathbf{x})^T \Phi_n^T (\Phi_n \Phi_n^T + \sigma^2 \mathbf{I})^{-1} \Phi_n \phi(\mathbf{x}), \quad (2.4)$$

which is equivalent to

$$\mu_n(\mathbf{x}) = \sigma^{-2} \phi(\mathbf{x})^T \Sigma_n \Phi_n^T \mathbf{y}_n, \quad \sigma_n^2(\mathbf{x}) = \phi(\mathbf{x})^T \Sigma_n \phi(\mathbf{x}), \quad \text{and } \Sigma_n = (\Phi_n^T \Phi_n \sigma^{-2} + \mathbf{I})^{-1}. \quad (2.5)$$

By the Woodbury matrix identity and the matrix determinant lemma, the log data likelihood becomes

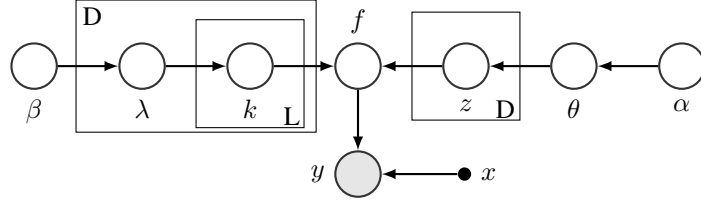
$$\log p(\mathcal{D}_n) = \frac{\sigma^{-4}}{2} \mathbf{y}_n^T \Phi_n \Sigma_n \Phi_n^T \mathbf{y}_n - \frac{1}{2} \log |\Sigma_n^{-1}| - \frac{\sigma^{-2}}{2} \mathbf{y}_n^T \mathbf{y}_n - \frac{n}{2} \log 2\pi\sigma^2. \quad (2.6)$$

For large scale observations, however, because the number of random features necessary to approximate the GP well in general increases with the number of observations [23], we cannot expect to solely use a fixed number of random features. Moreover, learning hyperparameters for random features is expensive: for Fourier features, the computation of Eq. (2.6) means re-computing the features, plus $O(D_R^3)$ for the inverse and determinant. With Mondrian features [17], we can learn the kernel width efficiently by adding more Mondrian blocks, but this procedure is not well compatible with learning additive structure, since the whole structure of the sampled Mondrian features will change. In addition, we typically need a forest of trees for a good approximation.

Tile coding Tile coding [27, 1] is a k -hot encoding widely used in the field of reinforcement learning as an efficient set of non-linear features. In its simplest form, tile coding is defined by k partitions, referred to as layers. An encoded data point becomes a binary vector with a non-zero entry corresponding to the each bin containing the data point. There exists methods for sampling random partitions which allow us to approximate various kernels, such as the ‘hat’ kernel.[21], making tile coding well suited for our application.

Variance starvation It is probably not surprising that using finite random features to learn the function *distribution* will result in a loss in accuracy [9]. For example, we observed that, while the mean predictions are preserved reasonably well around regions where we have observations, the confidence bound predictions can become very bad in regions where we do not have observations, once there are more observations than features. We refer to this underestimation of variance scale compared to mean scale, illustrated in Fig. 1, as ‘‘variance starvation’’.

Figure 2: The graphical model for TileGP, a Gaussian process with additive tiling kernels. The parameter λ controls the rate for the number of cuts k of the tilings (inverse of the kernel bandwidth); the parameter z controls the decomposition for the input space.



3 Ensemble Bayesian Optimization

Next, we describe an approach that can scale Bayesian Optimization when distributed computing resources are available. We name our approach, outlined in Algorithm 1, Ensemble Bayesian optimization (EBO). Our framework is inspired by the Mondrian forest, which partitions the search space via a Mondrian tree and aggregates the trees to a forest. In fact, Mondrian trees are even suitable to implement locality sensitive hashing. We use a (stochastic) series of Mondrian trees to partition the data, learn hyper-parameters for the kernel width its additive structure locally, and aggregate these parameters. Our forest hence spans across BO iterations.

In each iteration t of the optimization, we use a Mondrian process to randomly partition the search space into J parts (line 4), where J can be dependent on the size of the observations \mathcal{D}_{t-1} . In each part, we have a subset \mathcal{D}_{t-1}^j of observations. From those, we learn a local TileGP, a GP with probabilistic tile coding and additive structure, via Gibbs sampling (line 6). The probabilistic tile coding can be replaced by a Mondrian grid which approximates a Laplace kernel [3]. For parameter search problems, because experts design the loss function, we assume the availability of an upper bound on the function values. We use an acquisition function from [29, 28] which takes advantage of such bounds. Other BO strategies can also be used. Via the acquisition function, we generate a candidate set of points, and, from those, select a batch that is both informative (high-quality) and diverse (line 14). Since, in each iteration, we update the search space partition, the kernel width and the additive structure, the

algorithm may be viewed as implicitly running BO on an ensemble of GP models. In the following, we describe our model and the procedures of Alg. 1 in detail. We illustrate intuitively what EBO does in Fig. 4 when optimizing a 2D additive function (Fig. 3).

3.1 Gibbs Sampling for TileGP

We build on the additive GP with learned structure in [31], but greatly improve its efficiency by approximating each kernel $\kappa^{(m)}$ (supported on a subset of dimensions) by random features, essentially implementing a stochastic partition-based approximation along multiple axes. The random features are based on tile coding or Mondrian grids, with the number of cuts generated by D Poisson processes on $[0, R]$. Fig. 2 shows the graphical model of TileGP with fixed hyper-parameters α, β_0, β_1 ; the generative model is shown in Alg. 2.

Algorithm 1 Ensemble Bayesian Optimization (EBO)

```

1: function EBO ( $f, \mathcal{D}_0$ )
2:   Initialize  $z, k$ 
3:   for  $t = 1, \dots, T$  do
4:      $\{\mathcal{X}_j\}_{j=1}^J \leftarrow \text{MONDRIAN}([0, R]^D, z, k, J)$ 
5:     parfor  $j = 1, \dots, J$  do
6:        $z^j, k^j \leftarrow \text{GIBBSAMPLING}(z, k \mid \mathcal{D}_{t-1}^j)$ 
7:        $\eta_{t-1}^j(\cdot) \leftarrow \text{ACQUISITION}(\mathcal{D}_{t-1}^j, z^j, k^j)$ 
8:        $\{A_m\}_{m=1}^M \leftarrow \text{DECOMPOSITION}(z^j)$ 
9:       for  $m = 1, \dots, M$  do
10:         $\mathbf{x}_{tj}^{A_m} \leftarrow \arg \max_{\mathbf{x} \in \mathcal{X}_j^{A_m}} \eta_{t-1}^j(\mathbf{x})$ 
11:      end for
12:    end parfor
13:     $z \leftarrow \text{SYNC}(\{z^j\}_{j=1}^J), k \leftarrow \text{SYNC}(\{k^j\}_{j=1}^J)$ 
14:     $\{\mathbf{x}_{tb}\}_{b=1}^B \leftarrow \text{FILTER}(\{\mathbf{x}_{tj}\}_{j=1}^J \mid z, k)$ 
15:    parfor  $b = 1, \dots, B$  do
16:       $y_{tb} \leftarrow f(\mathbf{x}_{tb})$ 
17:    end parfor
18:     $\mathcal{D}_t \leftarrow \mathcal{D}_{t-1} \cup \{\mathbf{x}_{tb}, y_{tb}\}_{b=1}^B$ 
19:  end for
20: end function

```

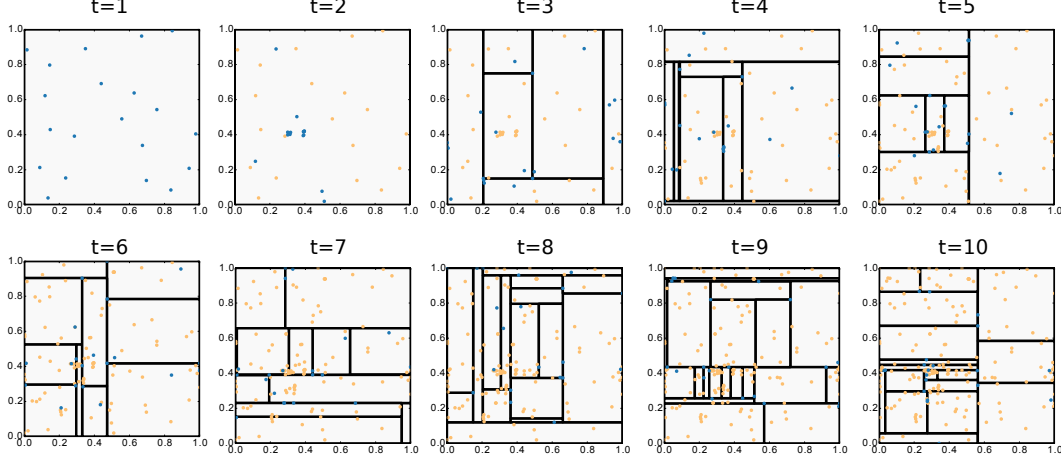


Figure 4: An example of 10 iterations of EBO on a 2D toy example where J is adaptive to the data size such that each leaf has at most 20 data points and B is set to be 20. The selections in each iteration is denoted in blue and the existing observations are in orange.

Tile coding samples the offset δ from a uniform distribution $U[0, \frac{R}{k_{di}}]$ and places the cuts uniformly starting at δ . The Mondrian grid samples k_{di} cut locations uniformly randomly from $[0, R]$.

Because of the data partition, we always have more features than observations, which can alleviate the variance starvation problem described in Section 2.

We can use Gibbs sampling to efficiently learn the cut parameter k and decomposition parameter z by marginalizing out both λ and θ . Notice that both k and z take discrete values, and doing Gibbs sampling means that we only needs to sample discrete variables, unlike other GP parameterizations.

Given the observations \mathcal{D}_n , the posterior distribution of the parameters λ, k, z, θ is

$$p(\lambda, k, z, \theta \mid \mathcal{D}_n; \alpha, \beta) \propto p(\mathcal{D}_n \mid z, k) p(z \mid \theta) p(k \mid \lambda) p(\theta; \alpha) p(\lambda; \beta). \quad (3.1)$$

Marginalizing over the Poisson rate parameter λ and the mixing proportion θ gives

$$p(k, z \mid \mathcal{D}_n; \alpha, \beta) \propto p(\mathcal{D}_n \mid z, k) \int p(z \mid \theta) p(\theta; \alpha) d\theta \int p(k \mid \lambda) p(\lambda; \beta) d\lambda \quad (3.2)$$

$$\propto p(\mathcal{D}_n \mid z, k) \frac{\Gamma(\sum_m \alpha_m)}{\Gamma(D + \sum_m \alpha_m)} \prod_m \frac{\Gamma(|A_m| + \alpha_m)}{\Gamma(\alpha_m)} \prod_d \frac{\Gamma(\beta_1 + |k_d|)}{(\prod_{i=1}^L k_{di}!) (\beta_0 + L)^{\beta_1 + |k_d|}} \quad (3.3)$$

where $|k_d| = \sum_{i=1}^L k_{di}$. Hence we only need to sample k and z when learning the kernel of TileGP. For each dimension d , we sample the group assignment z_d according to

$$p(z_d = m \mid \mathcal{D}_n, k, z_{-d}; \alpha) \propto p(\mathcal{D}_n \mid z, k) p(z_d \mid z_{-d}) \propto p(\mathcal{D}_n \mid z, k) (|A_m| + \alpha_m). \quad (3.4)$$

We sample the number of cuts k_{di} for each dimension d and the i -th from the posterior

$$p(k_{di} = j \mid \mathcal{D}_n, k_{-di}, z; \beta) \propto p(\mathcal{D}_n \mid z, k) p(k_{di} \mid k_{-di}) \propto \frac{p(\mathcal{D}_n \mid z, k) \Gamma(\beta_1 + |k_d|)}{(\beta_0 + L)^{k_{di}} k_{di}!}. \quad (3.5)$$

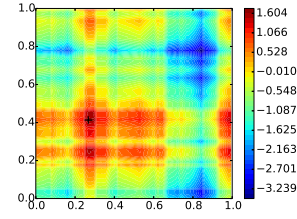


Figure 3: The 2D additive function we optimized in Fig. 4. The global maximum is marked with “+”.

3.2 Relations to Mondrian Kernels, Random Binning and additive Laplace Kernels

Our model described in Section 3.1 can use tile coding and Mondrian grids to construct the kernel. Tile coding and Mondrian grids are also closely related to Mondrian Features and Random Binning: all of the four kinds of random features attempt to find a sparse random-feature representation for the raw input \mathbf{x} based on the partition of the space with the help of layers. We illustrate the differences between one layer of the features constructed by tile coding, Mondrian grids, Mondrian features and random binning in Fig. 5.

For each layer of (our version of) tile coding, we sample a positive integer k (number of cuts) from a Poisson distribution parameterized by λR , and then set the offset to be a constant uniformly randomly sampled from $[0, \frac{R}{k}]$. For each layer of Mondrian grid, the number of cuts k is sampled the same as tile coding, but instead of using an offset and uniform cuts, we put the cuts at locations independently uniformly randomly from $[0, R]$. Random binning does not sample number of cuts k but samples the distance δ between neighboring cuts by drawing $\delta \sim \text{GAMMA}(2, \lambda R)$. Then, it samples the offset from $[0, \delta]$ and finally places the cuts. All of the above mentioned three types of random features can work individually for each dimension and then combine the cuts from all dimensions. For Mondrian features (Mondrian forest features to be exact), however, it partition the space jointly for all dimensions, and more details of Mondrian features can be found in [17, 4]. For all of these four types of random features and for each layer of the total L layers, the kernel is $\kappa_L(\mathbf{x}, \mathbf{x}') = \frac{1}{L} \sum_{l=1}^L \chi_l(\mathbf{x}, \mathbf{x}')$ where

$$\chi_l(\mathbf{x}, \mathbf{x}') = \begin{cases} 1 & \mathbf{x} \text{ and } \mathbf{x}' \text{ are in the same cell on the } l\text{-th layer} \\ 0 & \text{otherwise} \end{cases} \quad (3.6)$$

For the case where the kernel has M additive components, we simply use the tiling for each decomposition and normalize by LM instead of L . More precisely, we have $\kappa_L(\mathbf{x}, \mathbf{x}') = \frac{1}{LM} \sum_{m=1}^M \sum_{l=1}^L \chi_l(\mathbf{x}^{A_m}, \mathbf{x}'^{A_m})$.

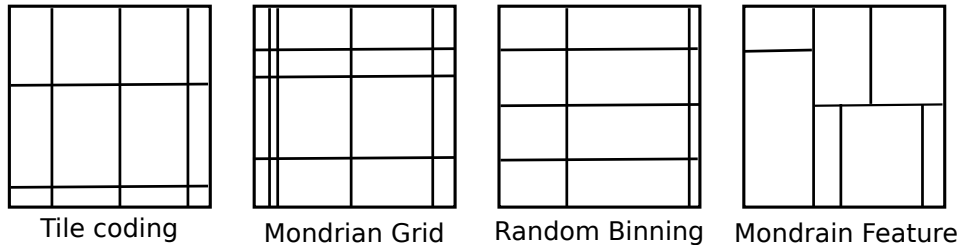


Figure 5: Illustrations of (our version of) tile coding, Mondrian Grid, random binning and Mondrian feature.

Mondrian grids, Mondrian features and random binning all converge to the Laplace kernel as the number of layers L goes to infinity. The tile coding kernel, however, does not approximate a Laplace kernel. Our model with Mondrian grids approximates an additive Laplace kernel:

Lemma 3.1. *Let the random variable $k_{di} \sim \text{POISSON}(\lambda_d R)$ be the number of cuts in the Mondrian grids of TileGP for dimension $d \in [D]$ and layer $i \in [L]$. The kernel of TileGP κ_L satisfies $\lim_{L \rightarrow \infty} \kappa_L(\mathbf{x}, \mathbf{x}') = \frac{1}{M} \sum_{m=1}^M e^{-\lambda_d R |\mathbf{x}^{A_m} - \mathbf{x}'^{A_m}|}$, where $\{A_m\}_{m=1}^M$ is the additive decomposition.*

Proof. When constructing the Mondrian grid for each layer and each dimension, one can think of the process of getting another cut as a Poisson point process on the interval $[0, R]$, where the time between

Algorithm 2 The generative model of TileGP

- 1: Draw mixing proportions $\theta \sim \text{DIR}(\alpha)$
 - 2: **for** $d = 1, \dots, D$ **do**
 - 3: Draw additive decomposition $z_d \sim \text{MULTI}(\theta)$
 - 4: Draw Poisson rate parameter $\lambda_d \sim \text{GAMMA}(\beta_0, \beta_1)$
 - 5: **for** $i = 1, \dots, L$ **do**
 - 6: Draw number of cuts $k_{di} \sim \text{POISSON}(\lambda_d R)$
 - 7: $\left\{ \begin{array}{ll} \text{Draw offset } \delta \sim U[0, \frac{R}{k_{di}}] & \text{Tile Coding} \\ \text{Draw cut locations } \mathbf{b} \sim U[0, R] & \text{Mondrian Grids} \end{array} \right.$
 - 8: **end for**
 - 9: **end for**
 - 10: Construct the feature projection ϕ and the kernel $\kappa = \phi^T \times \phi$ from z and sampled tiles
 - 11: Draw function $f \sim \mathcal{GP}(0, \kappa)$
 - 12: Given input \mathbf{x} , draw function value $y \sim \mathcal{N}(f(\mathbf{x}), \sigma)$
-

two consecutive cuts is modeled as an exponential random variable. Similar to Proposition 1 in [4], we have $\lim_{L \rightarrow \infty} \kappa_L^{(m)}(\mathbf{x}^{A_m}, \mathbf{x}'^{A_m}) = \mathbb{E}[\text{no cut between } \mathbf{x}_d \text{ and } \mathbf{x}'_d, \forall d \in A_m] = e^{-\lambda_d R |\mathbf{x}^{A_m} - \mathbf{x}'^{A_m}|}$.

By the additivity of the kernel, we have $\lim_{L \rightarrow \infty} \kappa_L(\mathbf{x}, \mathbf{x}') = \frac{1}{M} \sum_{m=1}^M e^{\lambda_d R |\mathbf{x}^{A_m} - \mathbf{x}'^{A_m}|}$. \square

Balog et al. [4] showed that in practice, the Mondrian kernel constructed from Mondrian features may perform slightly better than random binning in certain cases. Though it would be possible to use a Mondrian partition for each layer of tile coding, we only consider uniform, grid based binning with random offsets because this allows the non-zero features to be computed more efficiently ($O(1)$ instead of $O(\log k)$). Note that, as more dimensions are discretized in this manner, the number of features grows exponentially. However, the number of non-zero entries can be independently controlled, allow us to create sparse representations which are still computationally tractable.

3.3 Efficient data likelihood computation and parameter synchronization

We consider tile coding for our random features for their sparsity and efficiency properties. Since non-zero features can be found and computed by binning, the computational cost for encoding a data point scales linearly with dimensions and number of layers. In contrast, random Fourier basis only provide a dense representation and require far too many features for our application.

Since the number of non-zero features is quite small, we can efficiently compute a sparse Cholesky decomposition of the inner-product (Gram matrix) or the cross-product of the data. This allows us to efficiently compute the data likelihood given our feature representation.

In each iteration t , after the batch workers return the learned decomposition indicator z^b and the number of tiles $k^b, b \in [B]$, we synchronize these two parameters (line 13 of Alg. 1). For the number of tiles k , we set k_d to be the rounded mean of $\{k_d^b\}_{b=1}^B$ for each dimension $d \in [D]$. For the decomposition indicator, we use correlation clustering to cluster the input dimensions.

3.4 Filtering selections and budget allocation

In the EBO algorithm, we first use the batch workers to learn the local GPs and recommend potential good points from the local information. Then we aggregate the information of all the workers, and use a filter to select the points to evaluate from the set of points recommended by all the workers based on the aggregated information on the function.

There are two important details here: (1) how many points to recommend from each local worker (budget allocation); and (2) how to filter the selections. Usually in the beginning of the iterations, we do not have a lot of leaves (since we stop partitioning a leaf once it reaches the minimum leaf size). Hence, it is very likely that the number of leaves L is smaller than the size of the batch. Hence we need to allocate the budget of recommendations from each worker properly and use batch BO for each leaf. In our current version of EBO, we did the budget allocation using a heuristic, where we would like to generate at least $2B$ number of recommendations from all the workers, and each worker get the budget proportional to a score, the sum of the leaf volume (volume of the domain of the leaf) and the best function value of the leaf. For batch Bayesian optimization, we again uses a heuristic where points achieving the top n acquisition function values is always included and the other ones come from random points selected in that leaf.

Once we have all the recommended points, we select B number of them by maximizing another acquisition function whose domain is a batch of points: $\xi(X) = \log \det K_X + \sum_{b=1}^B \eta(\mathbf{x}_b)$ where $X = \{\mathbf{x}_b\}_{b=1}^B$. We use the log determinant term to force diversity and η to maintain quality. By the sub-modularity of the function ξ , we can optimize it greedily. Namely, we maximize $\xi(X \cup \{\mathbf{x}\}) - \xi(X) = \log(\kappa_{\mathbf{x}} - \kappa_{X\mathbf{x}}^T K_X^{-1} \kappa_{X\mathbf{x}}) + \eta(\mathbf{x})$ for B times. A similar approach can be found in [30].

3.5 Connections to evolutionary algorithms

Next, we make some observations that connect our randomized ensemble BO to ideas for global optimization heuristics that have successfully been used in other communities. In particular, these connections offer an explanation from a BO perspective and may aid further theoretical analysis.

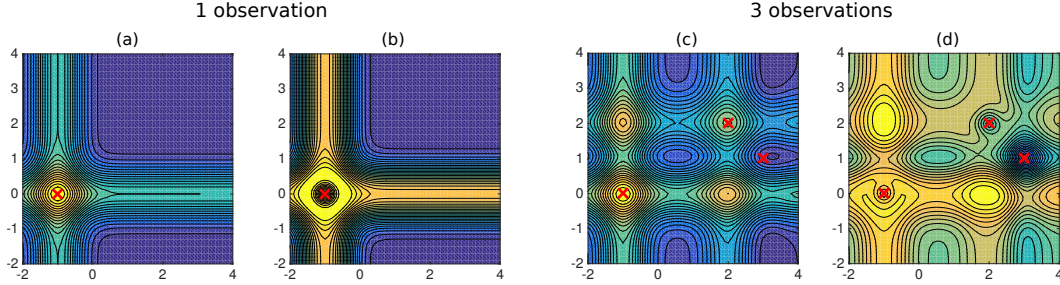


Figure 6: Posterior mean function (a, c) and GP-UCB acquisition function (b, d) for Add-GP in 2D. The maxima of the posterior mean and acquisition function are at the points resulting from exchange of coordinates between “good” points $(-1, 0)$ and $(2, 2)$.

Evolutionary algorithms [2] maintain an ensemble of “good” candidate solutions (called chromosomes) and, from those, generate new query points via a number of operations. These methods too, implicitly, need to balance exploration with local search in areas known to have high function values. Hence, there are local operations (mutations) for generating new points, such as random perturbations or local descent methods, and global operations. While it is relatively straightforward to draw connections between those local operations and optimization methods used in machine learning, we here focus on global exploration.

A popular global operation is *crossover*: given two “good” points $x, y \in \mathbb{R}^D$, this operation outputs a new point z whose coordinates are a combination of the coordinates of x and y , i.e., $z_i \in \{x_i, y_i\}$ for all $i \in [D]$. In fact, this operation is analogous to BO with a (randomized) additive kernel: the crossover strategy implicitly corresponds to the assumption that high function values can be achieved by combining coordinates from points with high function values. For comparison, consider an additive kernel $\kappa(x, x') = \sum_{m=1}^M \kappa^{(m)}(x^{A_m}, x'^{A_m})$ and $f(x) = \sum_{m=1}^M f^m(x^{A_m})$. Since each sub-kernel $\kappa^{(m)}$ is “blind” to the dimensions in the complement of A_m , any point x' that is close to an observed high-value point x in the dimensions A_m will receive a high value $f^m(x)$, independent of the other dimensions, and, as a result, looks like a “good” candidate.

We illustrate this reasoning with a 2D toy example. Figure 6 shows the posterior mean prediction and GP-UCB criterion $\hat{f}(x) + 0.1\sigma(x)$ for an additive kernel with $A_1 = \{1\}$, $A_2 = \{2\}$ and $\kappa^m(x_m, y_m) = \exp(-2(x_m - y_m)^2)$. High values of the observed points generalize along the dimensions “ignored” by the sub-kernels. After two good observations $(-1, 0)$ and $(2, 2)$, the “crossover” points $(-1, 2)$ and $(2, 0)$ are local maxima of GP-UCB and the posterior mean.

In real data, we do not know the best fitting underlying grouping structure. Hence, crossover does a random search over such partitions by performing random combinations, whereas our adaptive BO approach maintains a posterior distribution over partitions that adapts to the data.

4 Experiments

We empirically verify the scalability of EBO and its effectiveness of using random adaptive Mondrian partitions, and finally evaluate EBO on a real-world problem for a rover navigation task, where the goal is to maximize the value of the trajectory for a rover.

4.1 Scalability

We test the capacity of the Gibbs sampler of EBO with the state-of-the-art additive kernel learning algorithm, Structural Kernel Learning (SKL) from [31]. EBO can make use of the parallel resources both for Gibbs sampling and BO query selections, while SKL can only parallelize query selections but not the Gibbs sampler. Because the kernel learning part is the dominating factor of large scale BO, we compare the time each method need to run 10 iterations of Gibbs sampling with varying sizes of 20 dimensional observations from 100 to 50000. We show the timing results for the Gibbs samplers in Fig. 7(a), where EBO uses 240 cores via the Batch Service of Microsoft Azure. For EBO, the maximum number of leaves is set to be 1000 and the minimum leaf size is 100. Due to time limit, we did not finish SKL for more than 1500 observations. EBO runs more than 390 times faster

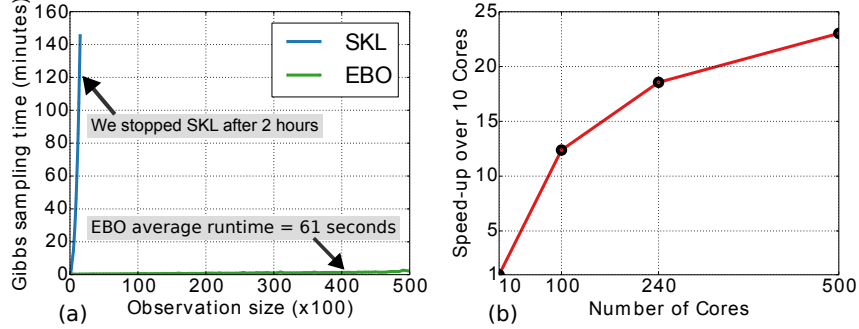


Figure 7: (a) Timing for the Gibbs sampler of EBO and SKL. EBO is significantly faster than SKL when the observation size N is relatively large. (b) Speed-up of EBO with 100, 240, 500 cores over EBO with 10 cores on 30,000 observations. Running EBO with 240 cores is almost 20 times faster than with 10 cores.

than SKL when the observation size is 1500. Comparing the quality of learned parameter z for the additive structure, SKL has a Rand Index of 96.3% and EBO has a Rand Index of 96.8%, which are similar on a toy example of fully partitioned function ($|A_m| = 1, \forall m$). We also show the speed-ups given different number of cores in Fig. 7(b). EBO with 500 cores is not significantly faster than with 240 cores because EBO runs synchronized parallelization, whose runtime is decided by the slowest core. It is often the case that most of the cores have finished while the program is waiting for the slowest 1 or 2 cores to finish.

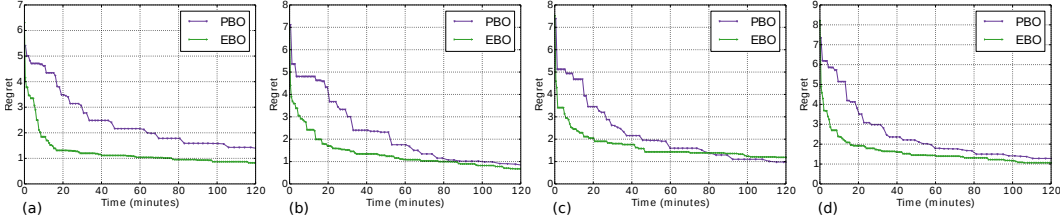


Figure 8: Comparing the regret of PBO and EBO on 4 different functions drawn from a 50D TileGP. EBO achieves lower regret than PBO in (a,b,d) and slightly higher regret than PBO in (c). In general, EBO finds a good point much faster than PBO.

4.2 Effectiveness of Mondrian ensembles

We verify the effectiveness of using ensemble models for BO on 4 functions randomly sampled from a 50-dimensional TileGP with known priors. In each iteration, the algorithm evaluates a batch of parameters of size B in parallel. We denote $\tilde{r}_t = \max_{x \in \mathcal{X}} f(x) - \max_{b \in [B]} f(x_{t,b})$ as the immediate regret obtained by the batch at iteration t , and $r_T = \min_{t \leq T} \tilde{r}_t$ as the regret, which captures the minimum gap between the best point found and the global optimum of the black-box function f . We compare Bayesian optimization with a fixed partition (PBO) against EBO with a randomly sampled partition in each iteration. PBO has the same 1000 leaves in all the iterations while EBO can have at most 1000 leaves. The decomposition parameter z and the kernel width parameter k are fixed to be the same as the TileGP prior to ensure a fair comparison. Our experimental results in Fig. 8 shows that EBO is able to find a good point much faster than PBO.

4.3 EBO for optimizing trajectories

To further explore the performance of our method, we consider a trajectory optimization task set in 2D meant to emulate a rover navigation task. We describe a problem instance by defining a start and goal position as well as a cost function over the state space. Trajectories are described by a set of points on which a BSpline is to be fitted. By integrating the cost function over a given trajectory, we can compute the total cost of a given solution. The goal is to find a trajectory with minimal total cost.

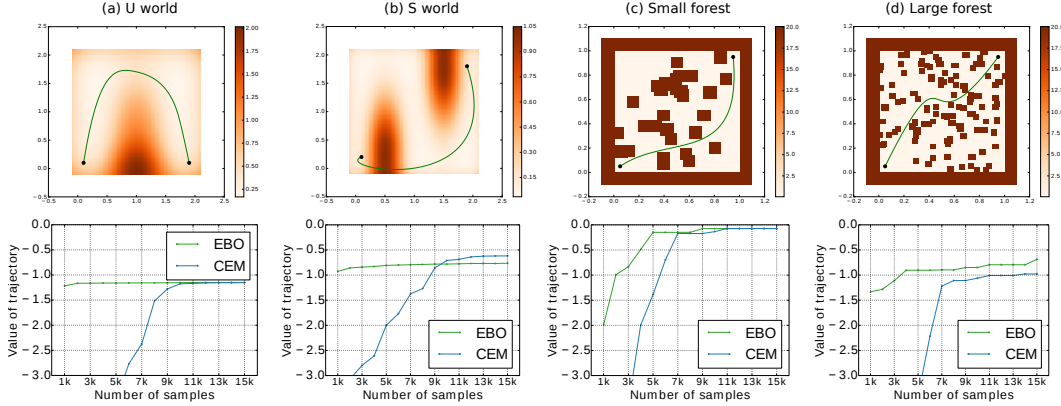


Figure 9: **Top row:** Rendering of an example trajectory in the different problem instances. The heat map corresponds to the cost function used. **Bottom row:** Plots of the value of best trajectory found given some number of evaluations. The value reported corresponds to the negative total cost of the trajectory.

In Figure 9, top row, we illustrate the four problem instance we’ve considered and provide an example trajectory. The ‘U World’, ‘S world’ and ‘small forest’ problems solve for a trajectory with 10 points making them a 20 dimensional optimization problem. The ‘large forest’ problem solves for a trajectory with 30 points making it 60 dimensional. In this settings, we set EBO to attempt to have Modriian partitions with fewer than 100 data points with a hard constraint of no more than 500 leaves. Each iteration evaluated the function on 1000 data points. Out of all the candidates, the top 500 candidate were evaluated based on the estimated value and 500 more were picked randomly.

We compare our approach to the cross-entropy method (CEM) and report the best solution found after a given number of evaluated trajectories. As seen in Figure 9, EBO reliably finds a near optimal solution in far fewer samples than CEM requires.

5 Discussion

5.1 Importance of avoiding variance starvation

Neural networks have been applied in many applications and received success for tasks including regression and classification. Researchers are still working on the theoretical understandings and one observation is that the success may come from overfitting [33]. Because the similarity between the test and training set in the reported experiments in, for example, the computer vision community, overfitting may seem to be less of a problem. However, in active learning (e.g. Bayesian optimization), we do not have a “test set”. We basically require the model to generalize well across the search space, and using the classic neural network may be detrimental to the data selection process, because of variance starvation (see Section 2). Gaussian processes, on the contrary, are good at estimating confidence bound and avoid overfitting. However, the scaling of Gaussian processes is hard in general. We would like to raise the attention of our community for the importance of the estimation of the confidence of the model predictions on new queries, a.k.a. avoiding variance starvation.

5.2 Future directions

Possible future directions include analyzing theoretically what should be the best input space partition strategy, batch worker budget distribution strategy, better ways of predicting variance in a principled way (not necessarily GP), better ways of doing small scale BO and how to adapt it to large scale BO. Moreover, add-GP is only one way of reducing function space, and there could be other better ones.

6 Conclusion

We propose a novel framework, ensemble Bayesian optimization, to tackle the scaling problem of Bayesian optimization. To achieve this, we proposed a new GP model based on tile coding and

additive structure. We also developed efficient Gibbs sampling approach to learn the latent variables. We demonstrate the capability of our method on high dimensional parameter search tasks for rover navigation with tens of thousands of observation data. Our empirical results showed that EBO is able to explore the space smartly and find better solutions than the cross-entropy method.

References

- [1] James S Albus et al. A new approach to manipulator control: The cerebellar model articulation controller (cmac). *Journal of dynamic systems, measurement and control*, 97(3):220–227, 1975.
- [2] Thomas Back. *Evolutionary algorithms in theory and practice: evolution strategies, evolutionary programming, genetic algorithms*. Oxford university press, 1996.
- [3] Matej Balog and Yee Whye Teh. The mondrian process for machine learning. *arXiv preprint arXiv:1507.05181*, 2015.
- [4] Matej Balog, Balaji Lakshminarayanan, Zoubin Ghahramani, Daniel M Roy, and Yee Whye Teh. The mondrian kernel. In *Uncertainty in Artificial Intelligence (UAI)*, 2016.
- [5] Roberto Calandra. *Bayesian Modeling for Optimization and Control in Robotics*. PhD thesis, Technische Universität, 2017.
- [6] Emile Contal, David Buffoni, Alexandre Robicquet, and Nicolas Vayatis. Parallel gaussian process optimization with upper confidence bound and pure exploration. In *Joint European Conference on Machine Learning and Knowledge Discovery in Databases*, pages 225–240. Springer, 2013.
- [7] Thomas Desautels, Andreas Krause, and Joel W Burdick. Parallelizing exploration-exploitation tradeoffs in Gaussian process bandit optimization. *Journal of Machine Learning Research*, 2014.
- [8] Josip Djolonga, Andreas Krause, and Volkan Cevher. High-dimensional Gaussian process bandits. In *Advances in Neural Information Processing Systems (NIPS)*, 2013.
- [9] Malcolm R Forster. Notice: No free lunches for anyone, bayesians included. *Department of Philosophy, University of Wisconsin–Madison Madison, USA*, 2005.
- [10] Javier González, Zhenwen Dai, Philipp Hennig, and Neil D Lawrence. Batch bayesian optimization via local penalization. *International Conference on Artificial Intelligence and Statistics (AISTATS)*, 2016.
- [11] Philipp Hennig and Christian J Schuler. Entropy search for information-efficient global optimization. *Journal of Machine Learning Research*, 13:1809–1837, 2012.
- [12] José Miguel Hernández-Lobato, Matthew W Hoffman, and Zoubin Ghahramani. Predictive entropy search for efficient global optimization of black-box functions. In *Advances in Neural Information Processing Systems (NIPS)*, 2014.
- [13] Kirthevasan Kandasamy, Jeff Schneider, and Barnabas Poczos. High dimensional Bayesian optimisation and bandits via additive models. In *International Conference on Machine Learning (ICML)*, 2015.
- [14] Kenji Kawaguchi, Leslie Pack Kaelbling, and Tomás Lozano-Pérez. Bayesian optimization with exponential convergence. In *Advances in Neural Information Processing Systems (NIPS)*, 2015.
- [15] Kenji Kawaguchi, Yu Maruyama, and Xiaoyu Zheng. Global continuous optimization with error bound and fast convergence. *Journal of Artificial Intelligence Research*, 56(1):153–195, 2016.
- [16] Harold J Kushner. A new method of locating the maximum point of an arbitrary multipeak curve in the presence of noise. *Journal of Fluids Engineering*, 86(1):97–106, 1964.
- [17] Balaji Lakshminarayanan, Daniel M Roy, and Yee Whye Teh. Mondrian forests for large-scale regression when uncertainty matters. In *Int. Conf. Artificial Intelligence Stat.(AISTATS)*, 2016.
- [18] Chun-Liang Li, Kirthevasan Kandasamy, Barnabás Póczos, and Jeff Schneider. High dimensional bayesian optimization via restricted projection pursuit models. In *International Conference on Artificial Intelligence and Statistics (AISTATS)*, 2016.
- [19] Mitchell McIntire, Daniel Ratner, and Stefano Ermon. Sparse Gaussian processes for bayesian optimization. In *Uncertainty in Artificial Intelligence (UAI)*, 2016.
- [20] J. Moćkus. On Bayesian methods for seeking the extremum. In *Optimization Techniques IFIP Technical Conference*, 1974.

- [21] Ali Rahimi, Benjamin Recht, et al. Random features for large-scale kernel machines. In *NIPS*, volume 3, page 5, 2007.
- [22] Carl Edward Rasmussen and Christopher KI Williams. Gaussian processes for machine learning. *The MIT Press*, 2006.
- [23] Alessandro Rudi, Raffaello Camoriano, and Lorenzo Rosasco. Generalization properties of learning with random features. *arXiv preprint arXiv:1602.04474*, 2016.
- [24] Jasper Snoek, Hugo Larochelle, and Ryan P Adams. Practical Bayesian optimization of machine learning algorithms. In *Advances in Neural Information Processing Systems (NIPS)*, 2012.
- [25] Jasper Snoek, Oren Rippel, Kevin Swersky, Ryan Kiros, Nadathur Satish, Narayanan Sundaram, Mostofa Patwary, Mr Prabhat, and Ryan Adams. Scalable bayesian optimization using deep neural networks. In *International Conference on Machine Learning*, 2015.
- [26] Niranjan Srinivas, Andreas Krause, Sham M Kakade, and Matthias W Seeger. Information-theoretic regret bounds for gaussian process optimization in the bandit setting. *IEEE Transactions on Information Theory*, 2012.
- [27] Richard S Sutton and Andrew G Barto. *Reinforcement learning: An introduction*, volume 1. MIT press Cambridge, 1998.
- [28] Zi Wang and Stefanie Jegelka. Max-value entropy search for efficient bayesian optimization. In *International Conference on Machine Learning (ICML)*, 2017.
- [29] Zi Wang, Bolei Zhou, and Stefanie Jegelka. Optimization as estimation with Gaussian processes in bandit settings. In *International Conference on Artificial Intelligence and Statistics (AISTATS)*, 2016.
- [30] Zi Wang, Stefanie Jegelka, Leslie Pack Kaelbling, and Tomás Lozano-Pérez. Focused model-learning and planning for non-gaussian continuous state-action systems. In *ICRA*, 2017.
- [31] Zi Wang, Chengtao Li, Stefanie Jegelka, and Pushmeet Kohli. Batched high-dimensional bayesian optimization via structural kernel learning. In *International Conference on Machine Learning (ICML)*, 2017.
- [32] Ziyu Wang, Frank Hutter, Masrour Zoghi, David Matheson, and Nando de Freitas. Bayesian optimization in a billion dimensions via random embeddings. *Journal of Artificial Intelligence Research*, 55:361–387, 2016.
- [33] Chiyuan Zhang, Samy Bengio, Moritz Hardt, Benjamin Recht, and Oriol Vinyals. Understanding deep learning requires rethinking generalization. In *International Conference on Learning Representations (ICLR)*, 2017.